Eddy Activity Sensitivity to Changes in the Vertical Structure of Baroclinicity

JANNI YUVAL AND YOHAI KASPI

Department of Earth and Planetary Sciences, Weizmann Institute of Science, Rehovot, Israel

(Manuscript received 12 May 2015, in final form 25 October 2015)

ABSTRACT

The relation between the mean meridional temperature gradient and eddy fluxes has been addressed by several eddy flux closure theories. However, these theories give little information on the dependence of eddy fluxes on the vertical structure of the temperature gradient. The response of eddies to changes in the vertical structure of the temperature gradient is especially interesting since global circulation models suggest that as a result of greenhouse warming, the lower-tropospheric temperature gradient will decrease whereas the upper-tropospheric temperature gradient will increase. The effects of the vertical structure of baroclinicity on atmospheric circulation, particularly on the eddy activity, are investigated. An idealized global circulation model with a modified Newtonian relaxation scheme is used. The scheme allows the authors to obtain a heating profile that produces a predetermined mean temperature profile and to study the response of eddy activity to changes in the vertical structure of baroclinicity. The results indicate that eddy activity is more sensitive to temperature gradient changes in the upper troposphere. It is suggested that the larger eddy sensitivity to the upper-tropospheric temperature gradient is a consequence of large baroclinicity concentrated in upper levels. This result is consistent with a 1D Eady-like model with nonuniform shear showing more sensitivity to shear changes in regions of larger baroclinicity. In some cases, an increased temperature gradient at lower-tropospheric levels might decrease the eddy kinetic energy, and it is demonstrated that this might be related to the midwinter minimum in eddy kinetic energy observed above the northern Pacific.

1. Introduction

Basic theory of linear baroclinic instability (Eady 1949) predicts that the growth rate of instabilities is proportional to

$$\lambda \propto \frac{g}{NT}\left|\frac{\partial T}{\partial y}\right|, \tag{1}$$

where λ is the (Eady) growth rate, N is the Brunt–Väisälä frequency, g is the acceleration due to gravity, T is the temperature, and y is the meridional direction. The Eady growth rate has been used extensively as a measure of the baroclinicity in climate systems. For example, Hoskins and Valdes (1990) used the Eady growth rate to quantify the geographical location and intensity of storm tracks. Despite the fact that the Eady growth rate provides a useful measure for baroclinicity, one should recognize its limitations. For example, considering the linear theory, Eq. (1) is valid in the case where the meridional temperature gradient divided by the temperature is constant with height, but in cases where it varies with height (nonuniform wind shear) Eq. (1) might be misrepresenting, and a theoretical prediction is missing. Furthermore, the dependence of eddy fluxes on the mean meridional temperature gradient has been addressed by various eddy flux closure schemes, such as those of Green (1970) and Held (1978). To derive such closure schemes, it was necessary to simplify the problem and assume that the vertical mean meridional temperature gradient is the relevant quantity, and not the vertical structure of the temperature gradient. Therefore, these closures do not predict the dependence of eddy fluxes on the vertical structure of the meridional temperature gradient.

Held and O'Brien (1992) were the first to study the effect of the vertical structure of the mean shear on eddy fluxes. They used a three-layer quasigeostrophic (QG) model, which is the simplest model possible to address this question since the wind shear in the two-layer model is constant. They concluded that for equal values of mean vertical shear, the eddy fluxes are greater when the shear is concentrated at the lower levels ($U_{zz} < 0$).

Corresponding author address: Janni Yuval, Department of Earth and Planetary Sciences, Weizmann Institute of Science, 234 Herzl St., Rehovot 7610001, Israel.
E-mail: yaniyuval@gmail.com

DOI: 10.1175/JAS-D-15-0128.1

Furthermore, they found that the eddy fluxes are more sensitive to the lower-level shear than to the upper-level shear, although the eddies were deeper in the case that the shear was concentrated in the upper layer. Pavan (1996), using a multilayer QG model, supported the results of Held and O'Brien (1992) and concluded that eddy activity (eddy fluxes, eddy kinetic energy) is more sensitive to the lower-level than to upper-level baroclinicity. Pavan (1996) interpreted this result as a consequence of the importance of shallow eddies in the dynamics. Later, Kodama and Iwasaki (2009) showed in aquaplanet experiments that wave activity is affected mainly by the lower-tropospheric temperature gradient. In a different study Iwasaki and Kodama (2011) showed that wave activity is also affected by an increased lower-stratospheric and upper-tropospheric temperature gradient, but the relative importance of upper and lower levels was not clear.

The effect of the vertical structure of baroclinicity on eddy activity has potentially important implication to atmospheric circulation during global warming. Global warming modeling experiments show a robust trend, where the equator-to-pole temperature difference in the lower levels of the atmosphere will decrease, while in the upper levels the tendency is opposite [Manabe and Wetherald (1975); Meehl et al. (2007), and see Vallis et al. (2014) for a model ensemble average of the temperature tendency from the fifth assessment report of the Intergovernmental Panel on Climate Change]. Consequently, the resulting baroclinicity tends to weaken in the lower troposphere but strengthen in the upper troposphere [this is mostly true in Northern Hemisphere winter—see Fig. 5 in Wu et al. (2011)].

The tropical warming aloft can be attributed to the decrease in the saturated lapse rate with increased water content following warming (Manabe and Wetherald 1980; Vallis et al. 2014). An increase in surface temperature of 1 K causes a decrease of approximately $0.1\,\mathrm{K\,km^{-1}}$ in the saturated lapse rate (Vallis et al. 2014). Therefore, for example, a surface warming of 1 K will cause double warming at a height of 10 km. This argument is valid for convective regions where the moist adiabatic lapse rate controls the temperature aloft, such as parts of the tropics. Since the horizontal temperature gradients at low latitudes are small (e.g., Sobel et al. 2001), the enhanced warming in the upper troposphere extends across the tropics. The large warming in the Arctic happens mostly in winter when the ice–albedo feedback is weak, and different studies showed in models that even without the ice–albedo effect polar amplification is present (e.g., Schneider et al. 1997; Alexeev 2003; Lu and Cai 2010). Cai (2005, 2006) suggested that polar amplification is caused by increased heat transport. Different studies by Hansen et al. (1984) and Bintanja et al. (2011) showed that the winter arctic warming near the surface is a result of large atmospheric static stability concentrated at low levels. Large static stability causes the polar atmosphere to emit a larger fraction of the longwave radiation downward (Bintanja et al. 2011), which warms the surface.

These temperature changes stem from robust thermodynamic effects and any feedbacks are unlikely to conceal them. These changes might lead to changes in the extratropical atmospheric circulation, such as a shift of the jet and storm tracks and changes in their intensity (e.g., Held 1993; Stephenson and Held 1993; Hall et al. 1994; Bengtsson and Hodges 2006; Yin 2005; O'Gorman and Schneider 2008; Wu et al. 2011; O'Gorman 2010). Changes in the location and amplitude of the storm track in response to global warming have significant impact on the poleward transport of heat, momentum, moisture, and on the hydrological cycle (Wu et al. 2011; O'Gorman 2015).

Lunkeit et al. (1998) used an idealized model with realistic temperature profiles to investigate the effects of global warming on atmospheric circulation and concluded that the lower-level baroclinicity will affect eddy activity more than upper-level baroclinicity. On the other hand, using a comprehensive climate model [the Geophysical Fluid Dynamics Laboratory Climate Model, version 2.1 (GFDL CM2.1)], Wu et al. (2011) investigated the effects of global warming on atmospheric circulation and concluded that the change in eddy kinetic energy (EKE) correlates better with the change in upper baroclinicity than the change in lower baroclinicity.

This paper aims to understand the effect of the vertical structure of baroclinicity on eddy activity, and more specifically to understand if baroclinic growth is dominated by the upper- or lower-level tropospheric baroclinicity. To do so, the vertical structure of the meridional temperature gradient is modified, and the response of eddies to such changes is investigated.[1] In this study two different approaches are taken to control the vertical structure of the meridional temperature gradient:

1) Changing the temperature field at different levels while keeping the temperature fixed at other levels (model setup is discussed in section 2c). In this method the relaxation temperature is prescribed to

[1] As demonstrated in the next sections, we find that EKE and eddy heat and momentum fluxes respond in a similar manner to modifications in baroclinicity and, therefore, throughout this paper we interchangeably use the terms EKE, eddy fluxes, and eddy activity. In general, eddy fluxes and EKE do not have the same response and in some cases can even have opposite trends (e.g., Ferrari and Nikurashin 2010).

produce a desired temperature field. To keep the temperature constant in all regions except in a chosen region, the relaxation temperature is modified in many regions and not only in the region where the temperature is modified. This method is similar in spirit to an eddy–mean flow interaction problem, where the mean state is (loosely) determined and the eddy response is investigated.

2) Changing the diabatic forcing with similar amplitude at different levels (model setup is discussed in section 2d). This is achieved by conducting experiments where the relaxation time τ is taken to be uniform in space and then modifying the relaxation temperature at different levels.

As both approaches are valid, in the next sections we use both approaches to investigate the effect of the vertical structure of baroclinicity on eddy activity. Both approaches show that eddy activity is affected significantly more by changes in the upper-tropospheric baroclinicity than lower-tropospheric baroclinicity.

The paper is arranged as follows. In section 2, the GCM and the methods used to alter the diabatic forcing in the model are discussed. In section 3, we present the results of different aspects of the circulation for different diabatic heating forcing used in the simulations. In section 4, a possible relation between our results to the midwinter minimum in EKE observed above the Pacific Ocean is presented. In section 5, we discuss different aspects of our results, and speculate why the upper-tropospheric temperature gradient has a larger effect on the eddy activity. It is demonstrated in a 1D Eady-like model that the instability growth rate is more sensitive to shear changes in levels that have larger shear than to changes in levels that have smaller shear. This suggests that the large effect of the upper baroclinicity on eddy activity is a result of larger baroclinicity in the upper levels. Conclusions are presented in section 6.

2. Methods

a. Model description

We use an idealized GCM based on the flexible modeling system of the National Oceanic and Atmospheric Administration (NOAA) GFDL. We work with a dry version of the model, which is driven by a Newtonian cooling scheme without orography or ocean, and unless stated differently at perpetual equinox. We use linear damping of near-surface winds with a damping rate of 1 day (Held and Suarez 1994) and a turbulent boundary layer scheme (roughness length of 5 cm) (Smagorinsky et al. 1965). These schemes represent turbulent dissipation in the planetary boundary layer in our simulations.[2] When a dry convection scheme is used, it is mentioned in the text, and a discussion and explanation of the convection scheme appears in section 2c. What distinguishes our simulations is the relaxation temperatures we use, which are different from the Held and Suarez (1994) relaxation temperature. The relaxation temperatures we use allow us to obtain any desired temperature profile (see section 2c for details).

The dynamical core of the idealized GCM is a hydrostatic spectral transform in vorticity-divergence form (Bourke 1974), with semi-implicit time differencing and a vertical σ coordinate. The spectral truncation is triangular, and the horizontal resolution we use is T42, corresponding to grid resolution of about $2.5° \times 2.5°$. The vertical discretization is based on a centered difference scheme, with 60 unequally spaced σ levels. The dynamical core of the idealized GCM is identical to the spectral dynamical core described by Held and Suarez (1994) and more details can be found there.

b. Diabatic forcing in the Newtonian relaxation scheme

The thermodynamic equation used in the idealized GCM, which is driven by a Newtonian cooling scheme is

$$\frac{DT}{Dt} = \frac{1}{\rho}\frac{Dp}{Dt} + \frac{T_{\text{relax}} - T}{\tau}, \tag{2}$$

where D/Dt is the material derivative that includes the nonlinear advection terms, T is the temperature, ρ is the density, p is the pressure, T_{relax} is the relaxation temperature that depends on latitude and pressure, and τ is the relaxation time that is also space dependent. The second term on the right-hand side is the diabatic heating as a result of Newtonian cooling.[3]

When using a Newtonian relaxation scheme, a common method to change the temperature field in a certain region is by modifying the relaxation temperature field at the desired region. This method is not

[2] We verified that the results presented here are qualitatively the same when using linear drag without the turbulent boundary layer scheme.

[3] The thermodynamic equation for the potential temperature can be expressed as $D\theta/Dt = Q$, where Q is the diabatic heating and $\theta = T(p_{\text{ref}}/p)^{\kappa}$ is the potential temperature. This means that the second term on the rhs of Eq. (2) $[(T_{\text{relax}} - T)/\tau]$ is proportional to $Q(p/p_{\text{ref}})^{\kappa}$.

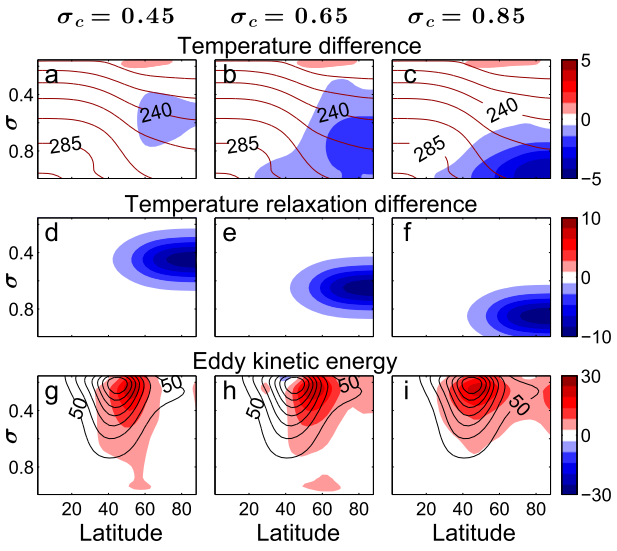

FIG. 1. (a)–(c) Change in the temperature field as a response to (d)–(e) changes in relaxation temperature at different levels and (g)–(i) EKE. Contours show the reference fields while colors show the deviation from the reference. The reference simulation used here is a simulation with the Held and Suarez (1994) parameters but includes a dry convection scheme with $\gamma = 0.7$. Contour intervals are 15 K for the temperature and 50 $m^2 s^{-2}$ for EKE.

satisfactory for our purposes for two main reasons. First, usually the relaxation time τ is a function of height and latitude (e.g., Held and Suarez 1994). Changing the relaxation temperature at different levels will cause different diabatic forcing and will cause very different temperature amplitude changes. Since we seek to study the effect of baroclinicity modifications at different levels on atmospheric circulation, the amplitude of the changes should be similar. Second, when the relaxation temperature is modified in one region, the temperature field is changed in many other regions, mainly as a result of advection. Generally, a linear relationship between T_{relax} and the time-mean temperature field $\hat{T}$ cannot be expected because the contribution of the nonlinear advection terms is large.

This is demonstrated in Figs. 1a–c, which show the temperature changes as a result of modifications in the relaxation temperature at different levels that are plotted in Figs. 1d–f. The temperature response at lower levels (Fig. 1c) is significantly larger than the temperature response to changes in the relaxation temperature at higher levels (Fig. 1a), and the induced temperatures changes at different levels are very different in magnitude. The EKE is plotted in Figs. 1g–i. Although the temperature gradient modifications in the lower levels are significantly larger than in the upper levels, the modification in the EKE is on the same order of magnitude. The reference simulation used in Fig. 1 is a simulation with the Held and Suarez (1994) parameters that includes a dry convection scheme with $\gamma = 0.7$.[4]

We conclude that in order to compare circulation changes as a result of changes in the vertical structure of baroclinicity, one should induce "similar changes" in the lower- and upper-tropospheric levels and investigate the circulation changes. The term similar changes is not uniquely defined and two such changes are investigated in this study (see description in sections 2c and 2d).

c. Controlling the temperature profile

In this section a method that permits simulations with a predetermined temperature field is presented. This method allows us to run simulations with different temperature fields, such that we change the temperature field in a chosen section of the atmosphere (in our case at certain vertical levels), while keeping the average temperature field at other levels approximately constant. This enables us to investigate the response of eddy activity to modifications in the vertical structure of the meridional temperature gradient field.

To simulate a desired temperature profile T_{target}, it is necessary to find T_{relax} [see Eq. (2)] that will produce the prescribed profile. The method we use is described below and is similar to the method used by Lunkeit et al. (1998).

1) The desired target temperature is chosen. The target temperature is the time- and zonal-mean temperature we wish the simulation to obtain. The different target temperatures investigated in this study are discussed below.
2) An iterative procedure is introduced to find the relaxation temperature that will approximately produce the desired target temperature field. The iterative equation for the relaxation temperature is

$$T_{\text{relax}}(t+\delta t) = T_{\text{relax}}(t) + \overline{\frac{T_{\text{target}} - T(t)}{\alpha}}, \qquad (3)$$

   where α is a dimensionless number chosen empirically, $T_{\text{relax}}(t+\delta t)$ denotes the relaxation temperature at time $t+\delta t$ where δt is one time step of the model, and $\overline{A}$ is a zonal average of a field A.
3) The relaxation temperature field $T_{\text{relax}}(t)$ obtained from the simulation is time averaged. This aver-

[4] The dry convection scheme assures that if an atmospheric column is less stable than a column with a temperature lapse rate of $\gamma\Gamma_d$, it relaxes temperatures toward a profile with a lapse rate of $\gamma\Gamma_d$ on a short time scale. The variable γ is a rescaling parameter and $\Gamma_d = g/c_p$ is the dry adiabatic lapse rate.

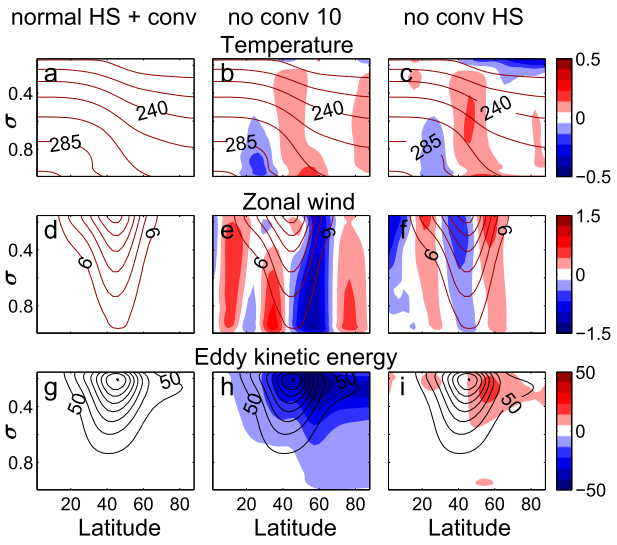

FIG. 2. (a)–(c) Temperature, (d)–(f) zonal wind, and (g)–(i) EKE for simulations in which the Held and Suarez (1994) forcing was used with a convection scheme and for two simulations that have the (nearly) same temperature field but with different relaxation times and no convection scheme. Contours show the fields of the simulation using the normal Held and Suarez parameters while colors show the deviation from this run. Contour intervals are 15 K for the temperature, 6 m s^{-1} for the zonal wind, and 50 m^2 s^{-2} for EKE.

aged field is time independent and used later in the idealized GCM experiments as the relaxation temperature. In our experiments we set $\alpha = 1500$, but the value has no importance as long as the relaxation temperature obtained produces a final temperature field similar to the target temperature.

This method can produce the relaxation temperature that will simulate any mean temperature profile with a very good accuracy (Figs. 2 and 3). Furthermore, using this method allows us to produce the same temperature profiles for different model parameters. For example, it is possible to use different relaxation temperatures that simulate the same temperature profile, where each relaxation temperature corresponds to a different set of model parameters, such as the relaxation time τ or convection scheme. Figure 2 shows the temperature, zonal wind, and the EKE for three simulations with similar temperature distribution. The left column in Fig. 2 describes the result of a simulation with the Held and Suarez (1994) parameters including a convection scheme ($\gamma = 0.7$). The middle and right columns are simulations obtained by using the method described in this section such that their target temperature T_{target} in Eq. (3) is the temperature field of the simulation in the left column of Fig. 2. The simulations in the middle and right columns do not include a convection scheme.

The difference between the simulations in the middle and right columns are the relaxation times, which are a uniform 10 days, and the Held and Suarez (1994) relaxation time, respectively, (with a relaxation time of 40 days in the upper atmosphere and 4 days in the equator surface). Although, the temperature distribution in these three simulations is very similar, the EKE differ substantially. Furthermore, the zonal wind in these simulations approximately follows thermal wind balance, and therefore the differences in the zonal wind occur due to surface effects (which cause whole columns to differ by approximately a similar amplitude). The simulations in the middle and right columns are used in the next sections as reference simulations.

To study the effect of the vertical structure of the temperature gradient on the eddy activity, the meridional temperature gradient of a reference run $\partial_y T_{\text{ref}}$ was modified in the extratropics, poleward of latitude 24°, in the following manner (Figs. 3d–f):

$$T_{\text{target}}(\mathbf{r}, |\phi| > 24) = T_{\text{ref}}(\mathbf{r}) + x[T_{\text{ref}}(\mathbf{r}) - T_{\text{ref}}(\mathbf{r}, |\phi| = 24)] \exp\left[-\frac{(\sigma - \sigma_c)^2}{2\delta\sigma^2}\right], \tag{4}$$

and unchanged at lower latitudes $[T_{\text{target}}(\mathbf{r}, |\phi| < 24) = T_{\text{ref}}(\mathbf{r})]$. The parameter T_{target} is the desired time-mean

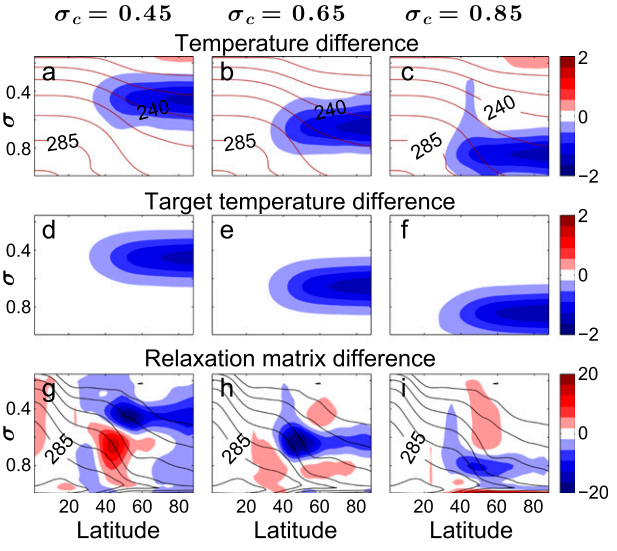

FIG. 3. (a)–(c) Temperature, (d)–(f) the theoretical desired temperature difference (T_{final} minus T_{ref}) calculated from Eq. (4), and (g)–(i) the modification in the relaxation temperature. In all plots the contours are values of the reference simulation, colors denote the deviation from reference, and the parameters used are $\delta\sigma = 0.1$, $x = 0.05$, and $\sigma_c = 0.45, 0.65, 0.85$. Contour intervals are 15 K for the temperature plots.

TABLE 1. Different parameters used in the presented simulations. Controlling temperature refers to the method described in section 2c. Controlling heating refers to the method described in section 2d.

Controlling temperature (relaxation time as in Held and Suarez 1994)	σ_c	Percentage change
	0.45	±0.02, ±0.05
	0.65	±0.02, ±0.05
	0.85	±0.02, ±0.05
	—	0 (Reference)
Controlling heating (uniform relaxation time 10 days)	σ_c	Amplitude change
	0.45	±1, ±2
	0.65	±1, ±2
	0.85	±1, ±2
	—	0 (Reference)
	0.1, 0.15, . . . , 0.9	±2

temperature field, **r** is latitude and is height dependent, σ is the vertical coordinate, σ_c is the vertical level where the maximal meridional temperature gradient is changed, $\delta\sigma$ determines the vertical interval of the temperature change, x determines the meridional temperature gradient percentage change, and $T_{\text{ref}}(\mathbf{r}, |\phi| = 24)$ is the reference temperature at latitude 24°.[5] In our simulations, T_{ref} is taken from a reference simulation using the Held and Suarez (1994) forcing including a convection scheme (see left panels in Fig. 2).

Unless stated differently, the parameters used in the simulations we present are $x = \pm 0.02, \pm 0.05$ for $\sigma_c = 0.45, 0.65, 0.85$ and $\delta\sigma = 0.1$ (see Table 1). These parameters allow us to study the effect of increased/decreased meridional temperature gradient in the extratropics at different levels on eddy activity. The reference simulation used when we compare the results of different simulations where the temperature profile was controlled in the next sections is a simulation in which the parameter $x = 0$ was used. This produces a similar temperature profile to the desired Held and Suarez (1994) temperature profile, and is presented in the right column of Fig. 2.

The simulations presented in sections 2 and 3 do not include a convection scheme (except for the simulations in Fig. 1 and the left column of Fig. 2). The underlying reason for this is that the static stability near the surface of the reference run is small, and when trying to modify the temperature gradient near the surface, the convection scheme "resists" this change, and does not allow these changes since the static stability is reduced below the convection threshold. To be able to change the temperature gradient at lower levels and be in a statically stable atmosphere, the reference temperature [T_{ref}, see Eq. (4)] was chosen to be the result of a simulation using the Held and Suarez (1994) forcing with a dry convection scheme parameter ($\gamma = 0.7$). We emphasize the fact that although the reference temperature used in Eq. (4) was obtained from a simulation in which a convection scheme was used, this does not mean that a convection scheme was used in the presented simulations. In section 4 the simulations presented include a convection scheme (see explanation in section 4).

Figure 3 shows the temperature difference $\overline{T}$ minus T_{ref} (Figs. 3a–c), the target temperature difference (Figs. 3d–f), and the relaxation temperature (Figs. 3g–i). The similarity between the target temperature and the mean temperature from the simulation confirms that this method can be used to simulate the desired changes from the reference simulation.

In the scheme described in this section, the vertical interval of the modifications applied to the temperature field was taken in σ coordinates. This choice changes the temperature for the same amount of mass in different levels. Another possibility is to change the temperature profile in such a way that the vertical interval of change will be similar in z coordinates. For a discussion and results of simulation using z coordinate interval see the appendix.

d. *Controlling the diabatic forcing*

A second approach we take to change the vertical structure of the meridional temperature gradient is by adding diabatic sources at different heights. These diabatic sources will modify the temperature field. The radiative diabatic forcing in the dry GFDL GCM is parameterized by two variables: a relaxation temperature and a relaxation time [τ in Eq. (2)]. As discussed in section 2b, in order to produce a similar change in the diabatic forcing in different levels it is necessary to account for the two. A simple way to add similar amplitude of diabatic heating is to change the relaxation temperature at different levels while taking a uniform relaxation time (τ = 10 days).[6]

[5] The reason the temperature field was modified poleward of latitude 24° is that we wanted to minimize changes in the tropical circulation that can also affect the extratropical circulation and focus on the question how the vertical structure of baroclinicity in the extratropics plays a role in the extratropical circulation.

[6] The diabatic forcing in the thermodynamic equation is $(T - T_{\text{relax}})/\tau$ (excluding friction), and itself depends on the temperature field. The mean temperature field in our simulations is known only after the simulation is performed. Therefore, the diabatic forcing change in our simulations is not equal in different simulations even when the relaxation time is uniform. This is because the temperature change magnitude is different in each simulation as a result of the advection terms.

Our reference run for this method is a run that has a similar temperature profile to Held and Suarez (1994) but with a uniform relaxation time of 10 days. To produce such a simulation, the scheme described in section 2c is used to find the relaxation temperature that produces this temperature profile with a uniform relaxation time. This simulation is presented in the middle column in Fig. 2.

The reference relaxation temperature was modified in the following way:

$$\delta T_{\text{relax}} = A\left\{1 + \tanh\left[\frac{3(|\phi| - \phi_b)}{\delta\phi}\right]\right\} \times \exp\left[\frac{-(\sigma - \sigma_c)^2}{2\delta\sigma^2}\right]\left(\frac{p}{p_{\text{ref}}}\right)^{\kappa}. \quad (5)$$

In the above, ϕ is latitude, ϕ_b controls the latitude where the change in the relaxation temperature saturates, $\delta\phi$ determines the sharpness of the gradient in the relaxation temperature, σ_c determines the level where the change in the relaxation temperature is maximal and A determines the amplitude of change in that relaxation temperature. The factor $(p/p_{\text{ref}})^{\kappa}$ is present in order to modify the diabatic forcing in a similar magnitude in the thermodynamic equation. The results presented in the next sections are for the parameter choice of $\phi_b = 50°$, $\delta\sigma = 0.1$, $\delta\phi = 45°$, $A = \pm 1$, ± 2 K, and $\sigma_c = 0.45$, 0.65, 0.85 unless stated differently (see Table 1). Figure 4 shows the relaxation temperature change (Figs. 4d–f) and the response of the temperature field to this change (Figs. 4a–c). This choice of parameters adds heating sources only in the extratropics and does not change the heating in the tropics. Different numerical values for the parameters were examined ($\phi_b = 33°$, $\delta\phi = 25°$, 90°, $\delta\sigma = 0.05$, 0.2), but the conclusions presented are invariant to the exact numerical values as long as the change in the relaxation temperature is concentrated at midlatitudes.

e. *Spinup details*

Every simulation presented ran for 5000 days and averaged over the last 4500 days where during each day the fields were taken four times a day. Hemispherically symmetric simulations were also averaged over the two hemispheres such that the presented plots of the Northern Hemisphere are actually an average over the two hemispheres (all simulations in section 3). Each experiment in the simulations that was used to obtain a relaxation temperature, ran for 8000 days and the relaxation temperature was obtained by averaging over the last 6000 days of the simulation.

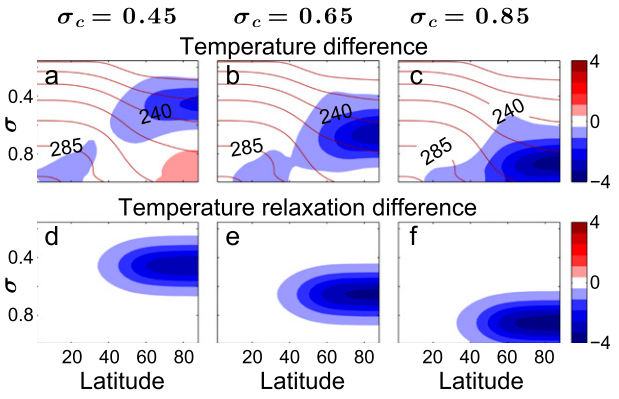

FIG. 4. (a)–(c) Temperature for simulations with different σ_c and $A = -2$ K and (d)–(f) modification in the relaxation temperature. Contours are values of the reference run while colors represent deviation from the reference. Contour intervals are 15 K for temperature.

3. The circulation response to changes in baroclinicity

In this section the response of the circulation and in particular the response of eddy activity to changes in the vertical structure of the meridional temperature gradient is investigated. In this study an eddy field is defined as the deviation from time and zonal mean, $A = \hat{\overline{A}} + A'$ where $\hat{A}$ is the time mean and $\overline{A}$ is the zonal mean of the field A. The modifications in the Eady growth rate and static stability caused by the temperature modifications are discussed in section 3a and the meridional barotropic shear response is discussed in section 3b. The eddy activity response to changes in the vertical structure of baroclinicity is discussed in section 3c, and in section 3d the changes in surface wind are discussed. We mostly concentrate on the differences between changes induced in the lower, middle, and upper troposphere and, therefore, the plots show in color the deviations from the reference simulations. In this section we use two different reference simulations for the two different methods described in sections 2c and 2d (see reference simulations in the right and middle columns of Fig. 2, respectively). Furthermore, the simulations are conducted for both cases of increased and decreased temperature gradients.

a. *Eady growth rate*

When changing the meridional temperature gradient at specific levels, the static stability changes as well. This is important since the baroclinicity is affected by both the meridional temperature gradient and the static stability. A simple approximate measure for the maximum baroclinic growth rate is given by Eq. (1).

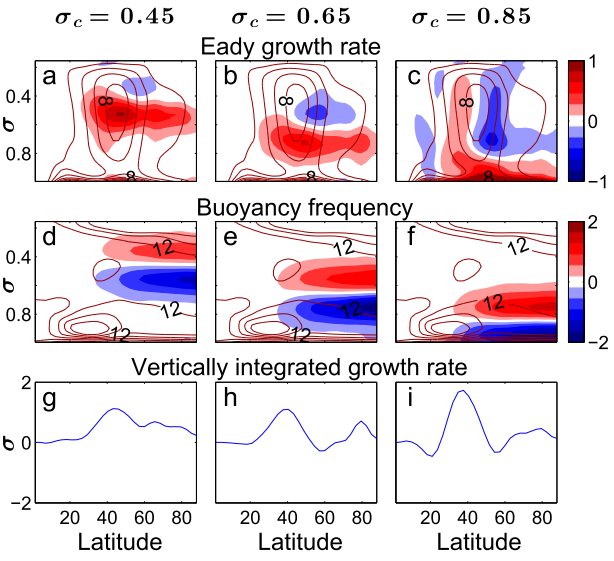

FIG. 5. (a)–(c) The Eady growth rate, (d)–(f) buoyancy frequency, and (g)–(i) vertically integrated Eady growth rate change for three different simulations where the level at which the meridional temperature gradient percentage change was $x = 0.05$ (method described in section 2c). Contours show the reference fields and colors show the deviation from the reference. Contour intervals are $2 \times 10^{-6}\,\mathrm{s}^{-1}$ for the Eady growth rate and $4 \times 10^{-3}\,\mathrm{s}^{-1}$ for the buoyancy frequency.

Although originating from linear theory, the Eady growth rate has been used extensively in the literature as a measure of baroclinicity (e.g., Ioannou and Lindzen 1986; Hoskins and Valdes 1990; Lorenz and Hartmann 2001; Merlis and Schneider 2009; Thompson and Barnes 2014). Figures 5 and 6 show the Eady growth rate (Figs. 5a–c and 6a–c), buoyancy frequency (Figs. 5d–f and 6d–f), and the vertically integrated Eady growth rate variation (Figs. 5g–i and 6g–i), defined as $\int \lambda\, d\sigma - \int \lambda^{\mathrm{ref}}\, d\sigma$ for simulations in which the temperature gradient was modified at different levels (Fig. 5), and in which the diabatic forcing was modified (Fig. 6). When increasing (decreasing) the meridional temperature gradient at certain levels the buoyancy frequency is modified such that above the maximal level of temperature change σ_c, the buoyancy frequency is increased (decreased) and below this level it is decreased (increased)—see Figs. 5d–f and 6d–f. As a result, the Eady growth rate is significantly increased (decreased) below σ_c because both the meridional temperature gradient and the buoyancy frequency are contributing to increase (decrease) the Eady growth rate. Above σ_c, the meridional temperature gradient and the buoyancy have an opposite effect on the Eady growth rate, and therefore its relative change is smaller. In sections 3b–e it is shown that the vertically integrated change of the Eady growth rate (Figs. 5g–i and 6g–i) is not predicting very well the net response of the eddies.

b. *Changes in the meridional shear—The barotropic governor*

When the vertical structure of the temperature profile is modified in our experiments, the meridional shear of the wind is also modified. It was demonstrated in many studies that changes in the barotropic meridional shear of the flow can affect baroclinic growth and barotropic conversion of eddies (e.g., James and Gray 1986; James 1987; Hartmann and Zuercher 1998; Chen et al. 2007). To understand if the eddy response in the experiments presented in this paper is mainly a result of changes in the vertical structure of baroclinicity or of changes in the meridional shear of the flow, the change in the amplitude of the barotropic (mean) shear ($|\int \partial_y u\, dp/\int dp| - |\int \partial_y u^{\mathrm{ref}}\, dp/\int dp|$) is shown in Fig. 7. In the case where the temperature profile was modified (Fig. 7a), the mean shear magnitude increase is largest when the upper troposphere is modified, which according to the barotropic governor mechanism, is expected to weaken the eddies. This mechanism is competing with the fact that the vertical shear was increased in these simulations. If the barotropic governor is playing an important role, it is expected that in the case of upper-tropospheric baroclinicity changes the eddy activity changes will be less than in the case of lower-/midtropospheric baroclinicity

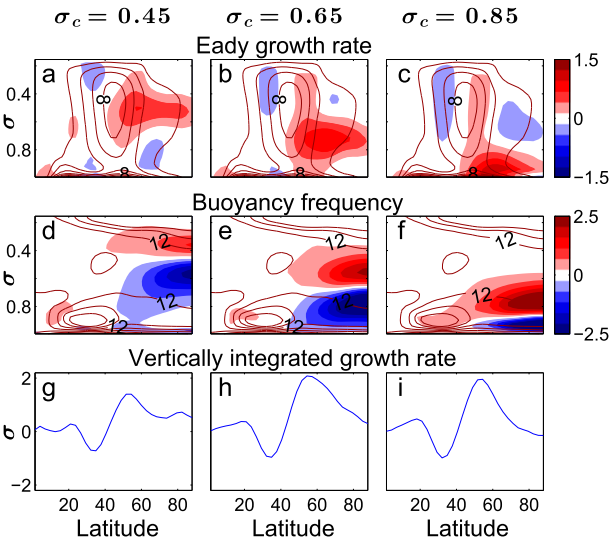

FIG. 6. (a)–(c) The Eady growth rate, (d)–(f) buoyancy frequency, and (g)–(i) vertical mean Eady growth rate for three different simulations where the level at which the diabatic heating was modified with $A = -2\,\mathrm{K}$ (method described in section 2d). Contours show the reference fields and colors show the deviation from the reference. Contour intervals are $2 \times 10^{-6}\,\mathrm{s}^{-1}$ for the Eady growth rate and $4 \times 10^{-3}\,\mathrm{s}^{-1}$ for the buoyancy frequency.

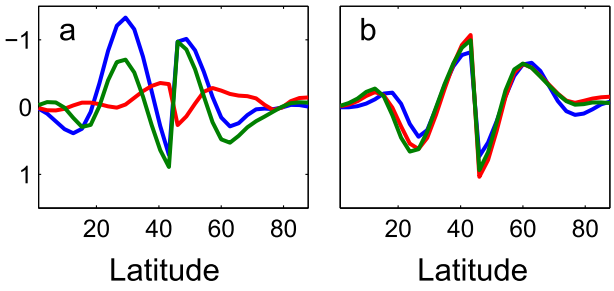

FIG. 7. The mean change in the barotropic (mean) shear magnitude ($10^{-6}\,s^{-1}$) for (a) the simulation where the temperature gradient was modified in different σ_c levels and a percentage change of $x = 0.05$ and (b) the simulation where the diabatic heating was applied in different σ_c levels and $A = -2$ K. Blue, red, and green are experiments using σ_c = 0.45, 0.65, and 0.85, respectively.

changes since the increased barotropic shear tend to decrease eddy activity. As demonstrated in sections 3c–e, the changes in eddy activity are largest when the upper baroclinicity is modified (Fig. 8), implying that the barotropic governor plays a less important role than the changes in the vertical structure of baroclinicity. In case the diabatic heating was controlled (Fig. 7b) the magnitude change in the barotropic shear in all simulations is very similar. As demonstrated in sections 3c–e, the changes in eddy activity are significantly larger when the heating in the upper troposphere is modified (Fig. 9), implying again, that in the simulations presented in this study, the changes in the barotropic shear play a smaller role in the eddy response than the vertical structure of baroclinicity.

c. *Eddy fluxes and eddy kinetic energy*

In Figs. 8 and 9, the eddy kinetic energy (Figs. 8a–c and 9a–c), eddy momentum flux (Figs. 8d–f and 9d–f), and eddy heat flux (Figs. 8g–i and 9g–i) are plotted for simulations where the temperature gradient was modified at different levels (Fig. 8) and for simulations where diabatic sources were added at different levels (Fig. 9).

When the temperature gradient (Fig. 8) or the diabatic heating gradient (Fig. 9) is increased in the upper troposphere, the eddy activity is modified significantly more than in cases where the temperature gradient (diabatic heating) is increased in the mid- or lower troposphere. Furthermore, the change in the eddy activity does not always follow the amplitude change of the Eady growth rate (Figs. 5g–i and 6g–i). For example, the eddy activity change is significantly larger when the diabatic sources are added in the upper troposphere than in the mid-troposphere (cf. Figs. 9a,d,g and 9b,e,h), but the vertically

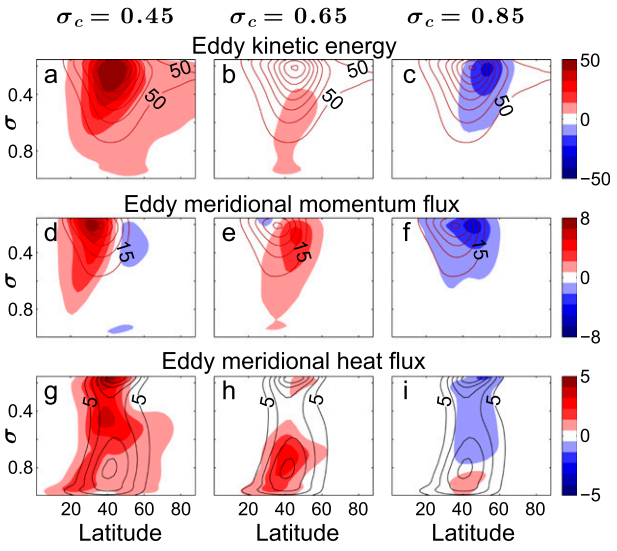

FIG. 8. (a)–(c) EKE, (d)–(f) eddy momentum flux, and (g)–(i) eddy heat flux for three different simulations where the level at which the meridional temperature gradient percentage change was $x = 0.05$ (method described in section 2c). Contours show the reference fields and colors show the deviation from the reference. Contour intervals are $50\,m^2\,s^{-2}$ for EKE, $15\,m^2\,s^{-2}$ for the momentum flux, and $5\,K\,m\,s^{-1}$ for the heat flux.

integrated Eady growth rate is larger when the diabatic sources are added in the midtroposphere than in the upper troposphere (Figs. 6g,h). This implies that the vertical structure has a significant effect on eddy activity.

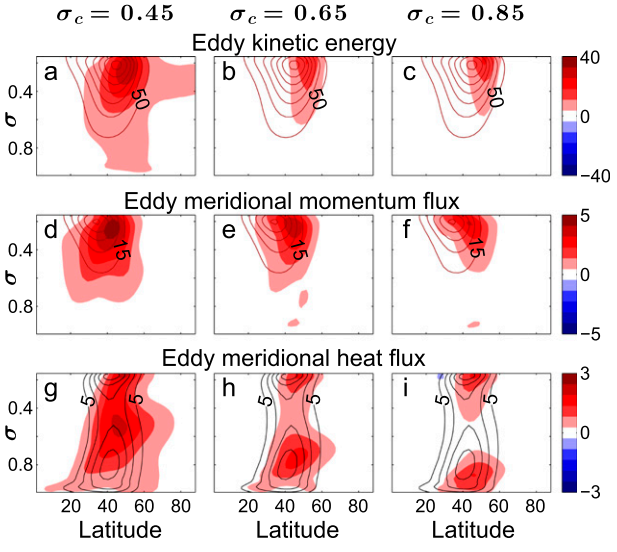

FIG. 9. (a)–(c) EKE, (d)–(f) eddy momentum flux, and (g)–(i) eddy heat flux for three different simulations where the diabatic heating was applied in different σ_c levels and $A = -2$ K. Contours show the reference fields while colors show the deviation from the reference. Contour intervals are $50\,m^2\,s^{-2}$ for EKE, $15\,m^2\,s^{-2}$ for the momentum flux, and $5\,K\,m\,s^{-1}$ for the heat flux.

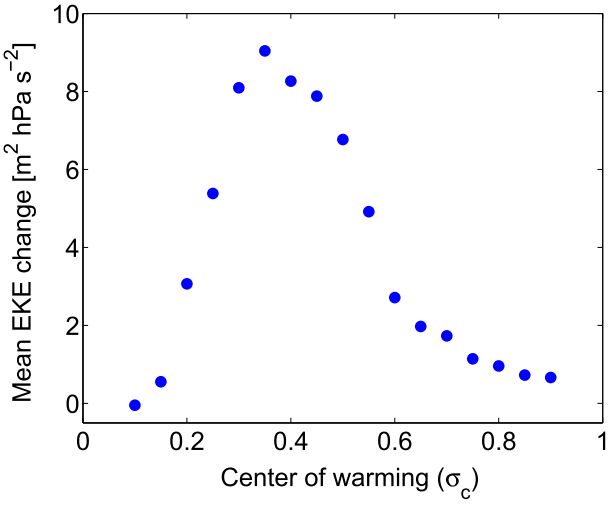

FIG. 10. The mean EKE change over the baroclinic zone $\left[\iint (u'^2 + v'^2) - (u'^2_{\text{ref}} + v'^2_{\text{ref}})\, d\phi\, dp\right]$ as a function of σ_c. The amplitude change in the diabatic heating is $A = -2$ K (see the description in section 2d).

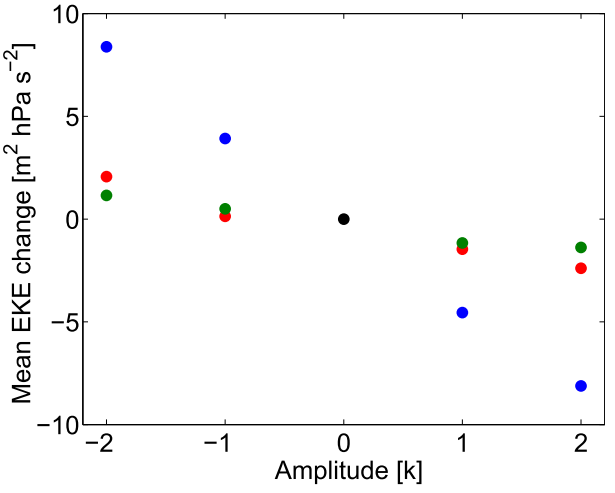

FIG. 11. The mean EKE change over the baroclinic zone $\left[\int_{27°}^{68°} \int (u'^2 + v'^2) - (u'^2_{\text{ref}} + v'^2_{\text{ref}})\, d\phi\, dp\right]$ as a function of the amplitude change in the diabatic heating (see the description in section 2d). The black dot represents the reference run. Blue, red, and green are experiments using $\sigma_c = 0.45$, 0.65, and 0.85, respectively.

Interestingly, when the baroclinicity is modified in the mid-/lower levels, the EKE response and eddy momentum flux response is maximal in the upper troposphere where it was maximal before the modification, and not at the level that the gradient was modified [see also discussion in Ait-Chaalal and Schneider (2015)]. On the other hand, the eddy heat flux response is maximal at the level where the gradient was modified, although the response is generally more barotropic than the changes in EKE and momentum flux.

Surprisingly, for the case where the temperature change is prescribed (Fig. 8), when the temperature gradient is increased in the lower troposphere, the EKE is decreased. This reduction in EKE as a response to the increase in meridional temperature gradient is not a robust effect and does not occur for all choices of the parameter $\delta\sigma$. This response also occurs in cases where the diabatic forcing is modified (as in section 2d) for certain parameter choices (e.g., $\phi_d = 90°$; not shown). Why a decreased temperature gradient in lower levels causes in certain cases an increased EKE requires further investigation and might be related to different factors, such as modification in the jet characteristics, static stability changes, or changes in the barotropic shear.[7] Nonetheless, such a decrease in EKE despite an increase in temperature gradients is also observed in nature during midwinter over the Pacific. This is further discussed in sections 4 and 5.

We next look at the change in the mean EKE over the baroclinic zone as a function of the level where the diabatic forcing was applied (Fig. 10) and as a function of the heating amplitude for simulations where the diabatic heating gradient was modified (Fig. 11).[8] When the heating is applied at the lower levels ($\sigma_c > 0.65$), the mean EKE slowly increases with decreasing σ_c (Fig. 10). As the heating is applied at higher levels in the troposphere, the change of the EKE increases rapidly with decreasing σ_c until the EKE reaches a maximum when $\sigma_c = 0.35$ (a little below the tropopause level). As the heating level is further increased above the tropopause ($\sigma_{\text{tropopause}} \approx 0.25$), the change in the EKE is reduced significantly. The EKE dependence on the diabatic heating amplitude in the amplitudes tested is roughly linear for a certain choice of σ_c (Fig. 11).

d. Zonal surface wind

Deviations from thermal wind balance appear mostly near the ground where surface friction is present. In the

[7] Changes in the barotropic shear are largest in the case that the upper troposphere is modified (Fig. 7), though the decrease in eddies is present when the lower baroclinicity is modified. Therefore, it is reasonable to assume that the barotropic shear is playing a smaller part than the vertical structure of baroclinicity in the changes of the eddy activity.

[8] The baroclinic zone is defined between the edge of the Hadley cell in our reference simulation (27° latitude) and 68° latitude. The results presented are not sensitive to changes in the definition of the baroclinic zone.

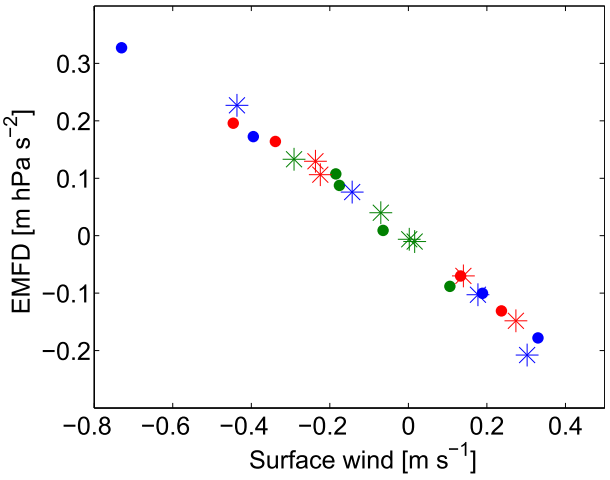

FIG. 12. Integrated eddy momentum flux divergence change $\left[\int \partial_y(v'u')\,dp - \int \partial_y(v'_{\mathrm{ref}}u'_{\mathrm{ref}})\,dp\right]$ as a function of surface wind change at the latitude of maximal wind divergence. The asterisks are from predetermined temperature experiments (section 2c) and the dots are from diabatic heating modifications experiments (section 2d). Blue, red, and green are experiments using $\sigma_c = 0.45$, 0.65, and 0.85, respectively.

Ferrel cell, the surface wind is predicted to be proportional to the integrated eddy momentum divergence (Vallis 2006). Figure 12 shows the relation between the maximum of eddy momentum divergence change to the change of the surface wind for simulations where the temperature or diabatic heating was added at different levels.[9] The figure shows that there is a linear relation between the surface wind change and the vertically integrated momentum flux divergence change. Furthermore, it shows that in cases where the upper-tropospheric baroclinicity is modified, the response of the surface wind is larger (compare the blue asterisks and dots with the red and green asterisks and dots). These results indicate that the surface zonal wind is mostly affected from upper-tropospheric changes since the eddy activity is affected mostly from upper meridional temperature gradient.

e. *MAPE and EKE*

Previous studies found that the mean available potential energy (MAPE) and EKE scale together (e.g., O'Gorman and Schneider 2008). To investigate if the sensitivity of EKE to changes in the upper-tropospheric temperature gradient are as a result of larger changes in MAPE, the relation between MAPE change (MAPE minus $\mathrm{MAPE}_{\mathrm{ref}}$) and EKE change is plotted for different simulations in Fig. 13. MAPE is calculated using the quadratic approximation of Lorenz (1955) in sigma coordinates. Following O'Gorman and Schneider (2008), we exclude levels below $\sigma_s = 0.9$ and above the troposphere and calculate MAPE in the baroclinic zone defined here between 27° and 68°. The qualitative results we present are insensitive to different choices of baroclinic zones. The resulting expression for MAPE per unit area is

$$\mathrm{MAPE} = \int_{\sigma_t}^{\sigma_s} \frac{c_p p_0}{2g} \Gamma \left(\frac{\langle \overline{p} \rangle}{p_0}\right)^{\kappa} (\langle \overline{\theta}^2 \rangle - \langle \overline{\theta} \rangle^2)\, d\sigma, \qquad (6)$$

where $\overline{A}$ is the zonal time mean of field A, $\langle A \rangle$ is the average over the baroclinic zone, σ_t is the tropopause height in the baroclinic region, c_p is the heat capacity, g is the gravity acceleration, $p_0 = 10^5$ Pa is a reference surface pressure, and θ is the potential temperature. The factor Γ is an inverse measure of dry static stability:

$$\Gamma = -\frac{\kappa}{\langle \overline{p} \rangle} \left\langle \frac{\partial \overline{\theta}}{\partial p} \right\rangle^{-1}. \qquad (7)$$

In contrast to the results of O'Gorman and Schneider (2008), it is found that when the baroclinicity in modified in different layers, the relation between the MAPE change and the EKE change does not have a linear relation. Despite this, when examining each set of experiments separately, namely, each method (dots or

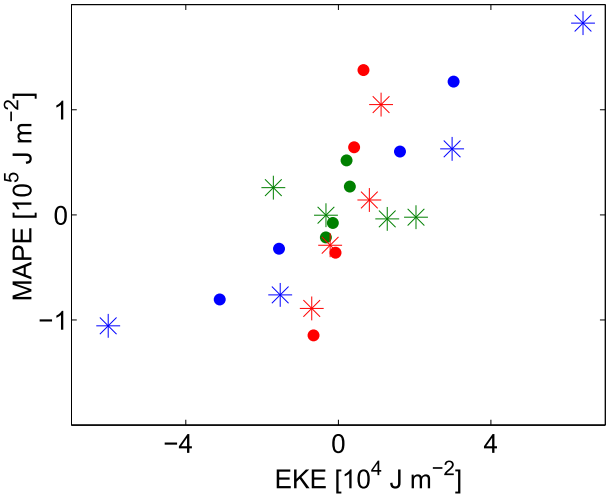

FIG. 13. MAPE change as a function of EKE change. The asterisks are from predetermined temperature experiments (section 2c) and the dots are from diabatic heating modifications experiments (section 2d). Blue, red, and green are experiments using $\sigma_c = 0.45$, 0.65, and 0.85, respectively.

[9] The surface wind is defined as an average over the lower three levels of the model, and calculating the zonal wind and the momentum divergence as a meridional average of ±7.5° around the maximum in the divergence.

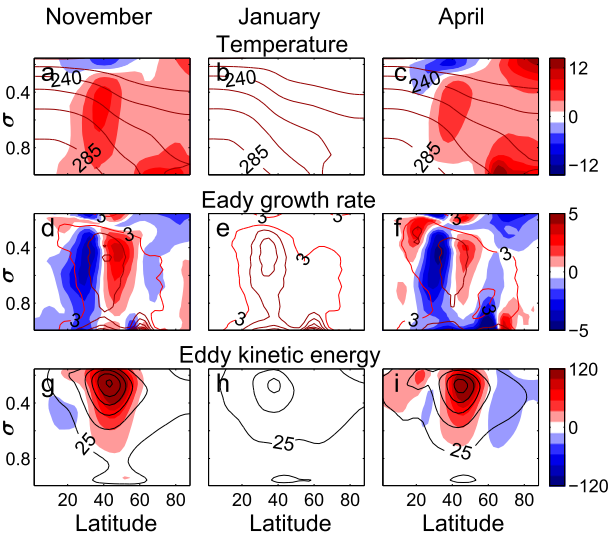

FIG. 14. (a)–(c) Temperature, (d)–(f) Eady growth rate, and (g)–(i) the EKE for November, January, and April simulations. Contours represent the values of the presented month while colors show the difference from January. Contour intervals are 15 K for temperature, $3 \times 10^{-6}\,s^{-1}$ for the Eady growth rate, and $50\,m^2\,s^{-2}$ for EKE.

asterisks) and level of baroclinicity change (color), there is an approximate linear relation between MAPE and EKE. This implies that there is a relation between MAPE and EKE, though the vertical region where MAPE is modified plays a major role in determining the effect on EKE change. Furthermore, when the temperature is modified in the lower troposphere (green asterisks) there is an opposite relation between MAPE and EKE, which is consistent with the results shown in Fig. 8 (for further discussion see also sections 3c and 4).

4. Possible relation to the Pacific midwinter minimum

The results presented in section 3c showed that in some cases when the temperature gradient increases (decreases) in the lower troposphere, a decrease (increase) in the EKE is seen. This is opposite to what is predicted from linear theory, where instabilities (and hence EKE) are expected to strengthen with increased temperature gradient and jet strength [see Eq. (1)]. Nevertheless, such an increased temperature gradient that is accompanied with a decrease in EKE is observed on Earth during midwinter above the northern Pacific Ocean (Nakamura 1992). This is counterintuitive since the meridional temperature gradient is largest in January, but EKE is at a local minimum during midwinter. There have been several proposed mechanisms for this phenomena (e.g., Chang 2001; Harnik and Chang 2004; Penny et al. 2010; Park et al. 2010).

We investigate in this section a possible connection between the midwinter minimum and the results presented in Fig. 8, which show that in certain cases an increased temperature gradient might lead to a decrease in the EKE. First, it is verified that the midwinter minimum can be reproduced using our idealized GCM. This is done by using the method described in section 2c, which allows simulating the observed mean temperature profile above the Pacific Ocean in November, January, and April (Figs. 14a–c).

The target temperature profiles for the different months were determined by averaging the NCEP–NCAR reanalysis temperature data between the years 1981 and 2010 separately for each month of the climatology. Focusing on the Pacific basin we zonally averaged the data over longitudes above the Pacific (160°E–138°W) such that the target temperature is zonally symmetric. The temperature profiles we got are very similar to the target temperature (maximal deviation from the target temperature is less than 1 K). The relaxation time in these simulation was 4 days for the tropic surface as in Held and Suarez (1994) and 20 days in the upper part of the atmosphere, which is half compared to the one used in Held and Suarez (1994).[10] Furthermore, A dry convection scheme with $\gamma = 0.9$ was used. The reason this convection scheme is used in these simulations is because the mean temperature profile in the simulations that include a convection scheme had a better agreement with the target temperature. When a convection scheme is not included, the qualitative conclusions are similar though there are larger deviations from the target temperature.

When the different temperatures profiles above the Pacific are simulated, a minimum in EKE is present in January (Figs. 14g–i). The fact that a minimum in EKE appears in our simulations when using a January temperature profile, is an indication that the diabatic heating, which creates this temperature profile, is a key factor to the presence of the minimum in our simulations. We stress that though the temperature field in our simulations reproduce the mean

[10] Also a uniform 7-day relaxation time and the relaxation time used in Held and Suarez (1994) were simulated and produced similar trends. The reason the relaxation temperature from Held and Suarez (1994) was modified is that one needs to run a much longer simulations in order to produce the target temperature profile accurately when using a long relaxation time in the upper troposphere as in Held and Suarez (1994). When using a uniform relaxation time of 7 days, the temperature in the simulation is more similar to the target temperature (less than 0.5-K difference), but EKE is much smaller due the fast relaxation in the upper troposphere.

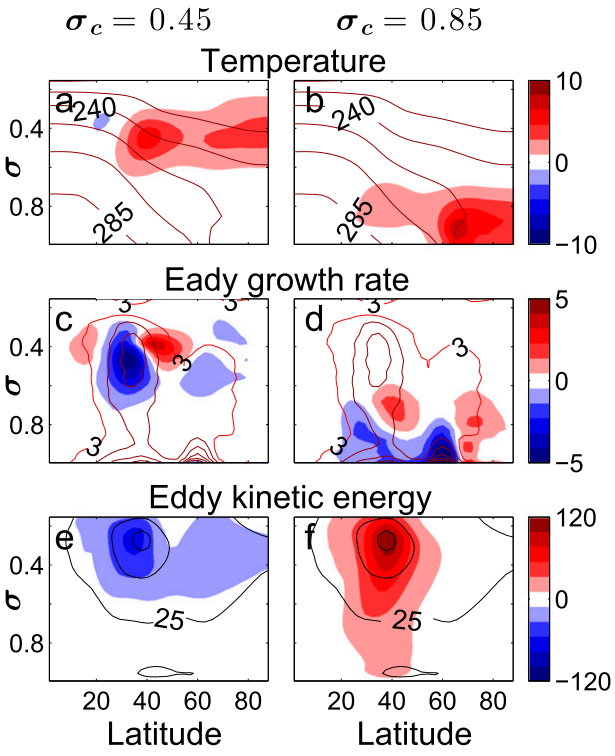

FIG. 15. (a)–(c) Temperature, (d)–(f) Eady growth rate, and (g)–(i) EKE using the target temperature from Eq. (8) with σ_c = 0.45, 0.85. Contours represent the value of January fields and colors show the difference from January. Contour intervals are 15 K for the temperature, $3 \times 10^{-6}\,\mathrm{s}^{-1}$ for the Eady growth rate, and $50\,\mathrm{m}^2\,\mathrm{s}^{-2}$ for the EKE.

temperature profile above the northern Pacific very accurately, the wind profile is different from observations due to surface winds that are not reproduced (away from the ground wind obey thermal wind relation). Furthermore, the EKE amplitude we obtain is different in magnitude from the observed one. When comparing the 3–10-day bandpass filter of the EKE calculated from reanalysis data to the simulations presented in this paper (not shown), we find that EKE obtained from the reanalysis data is larger (by a factor of 1.5–2). Chang (2006) found a similar trend and explained it by the fact that the mean state is neutrally stable (Hall and Sardeshmukh 1998), and therefore eddies are relatively weak in the simulations. It is worth mentioning that the magnitude of EKE is strongly dependent on the choice of relaxation time, and different choices of relaxation times tend to change the frequencies at which EKE peaks. Despite these differences, the main conclusion here relies on the fact that the trend in EKE in our simulations shows a similar trend as in observations.

Next, in order to study the role of the lower/upper temperature gradient change in the emergence of the minimum, the January temperature profile is modified, such that the lower or upper temperature field is taken to be April-like. Namely,

$$T_{\mathrm{target}} = T_{\mathrm{Jan}} + (T_{\mathrm{Apr}} - T_{\mathrm{Jan}}) \exp\left[\frac{-(\sigma - \sigma_c)^2}{2\delta\sigma^2}\right], \quad (8)$$

where T_{Jan} and T_{Apr} are the mean temperature fields above the Pacific in January and April, respectively. When $\sigma_c = 0.85$ ($\sigma_c = 0.45$), the lower (upper) temperature field is modified to be April-like while the other levels are January-like. Figure 15 shows the temperature profile, Eady growth rate, and EKE for simulations using the target temperature from Eq. (8). Notice that the EKE is increased when the lower-tropospheric temperature gradient is decreased, and it is decreased when the upper temperature profile is modified (compared to normal January). This result is consistent with the results shown in Fig. 8 where EKE decreased (increased) when the temperature gradient increased in the lower- (upper-) tropospheric levels. The results from Fig. 15 suggest that a possible contribution to the midwinter minimum is an increased temperature gradient in lower-tropospheric levels during midwinter (or alternatively, the modification in the lower-tropospheric temperature field). The increase in the lower-tropospheric temperature gradient is probably not the sole reason for the minimum seen in our simulations, and other contributions such as increased static stability and the fact that in some regions the temperature gradient increases (although the mean decreases), might play an important role.

5. Discussion

a. *Why upper baroclinicity affects more eddy activity*

The Eady growth rate[11] of the reference simulations is plotted in Figs. 5a and 6a. The maximum Eady growth rate of our reference state occurs at midlatitudes at a height of $\sigma \approx 0.45$. One possible reason for the large effect of the upper baroclinicity on eddy activity is that when modifying the temperature gradient at upper-tropospheric levels, the region with maximal Eady growth rate is modified. If the most important region for growth of instabilities is the region where the Eady growth rate is maximal locally, then we

[11] In the following discussion we refer to the Eady growth rate as the growth rate calculated from the standard Eady problem for every grid point as calculated in Eq. (1). In previous sections the Eady growth rate was used as a baroclinicity measure.

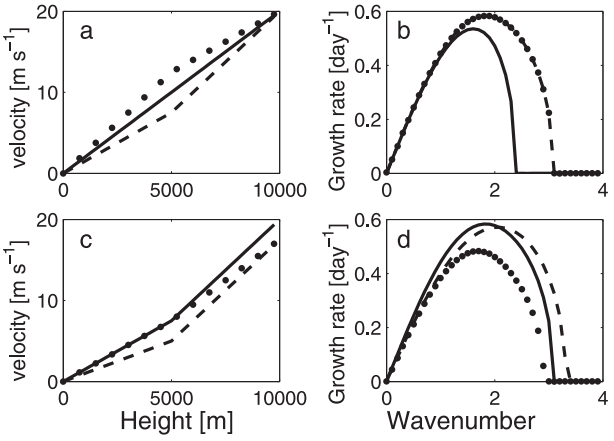

FIG. 16. (a),(c) The vertical profile of the zonal wind specified to the 1D Eady-like problem. (b),(d) Growth rate as a function of rescaled wavenumber [$k^* = (Nh_2/f)k$] for the 1D modified problem corresponding to the velocities in (a) and (c), respectively. The solid, dashed, and dotted lines are the reference shear, decreased lower shear, and decreased upper shear, respectively.

expect that the largest effect on eddy activity will be when this region's baroclinicity is modified. On the other hand, according to this hypothesis, modifying the temperature gradient at mid-/lower-tropospheric levels, changes the Eady growth rate at tropospheric levels where the Eady growth rate is small, and therefore there is a weaker eddy response. To test this hypothesis, we develop a simple 1D Eady-like problem with piecewise linear shear and demonstrate that indeed changes in the regions of maximal shear (i.e., maximal Eady growth rate) are those that have the largest effect on the growth rate.

One-dimensional Eady-like models were shown to be useful in various cases, for example, to study the effect of stratospheric shear on instabilities (Wittman et al. 2007; Muller 1991), and the effect of changes in the static stability on instabilities (Blumen 1979). Here it is demonstrated that if the shear is not uniform across the atmosphere, shear modifications in the layer that has a larger shear has a larger effect on the growth rate than shear modifications in the layer that has a smaller shear. In section 3 it was demonstrated that changes in the temperature gradient in upper levels of the troposphere, where the Eady growth rate is larger, affect more eddy activity than temperature gradient changes in lower levels where the Eady growth rate is smaller. Although baroclinicity measures (such as the Eady growth rate) depend on both the shear and the static stability, in the Eady-like problem solved here only the wind shear is modified. Since the buoyancy frequency is constant in this 1D Eady-like problem, shear modifications are analogous to Eady growth-rate changes in the GCM simulations. Furthermore, the calculated growth rate in the 1D Eady-like problem is analogous to the eddy activity in the simulations.

We consider two atmospheric sections, equal in depth, in which the static stability N, density, and wind shear are constant in each one of them. The two levels represent the upper and lower troposphere, and they differ only in their wind shear (γ_l, γ_u where subscript l and u are for the lower and upper levels, respectively). Since the Eady problem is well known, and a comprehensive mathematical development of the 1D QG Eady problem is given in standard textbooks (e.g., Pedlosky 1987; Vallis 2006), we give here only a short description of the mathematical equations. The troposphere is bounded below at $z = 0$. The two levels share a free interface at $z = h_1$, and the troposphere is bounded from above at $z = h_2$. We write the equations in terms of nondimensional parameters: the horizontal coordinate $x^* = (f_0/Nh_1)x$, time $t^* = (f_0\gamma_l/N)t$, vertical coordinate $z^* = (1/h_1)z$, nondimensional shear parameter $\gamma^* = \gamma_u/\gamma_l$, and a nondimensional height parameter $h^* = h_2/h_1$, where f_0 is the Coriolis parameter and the starred parameters are dimensionless. The streamfunction in each layer obeys the QG potential vorticity equation, which can be expressed as the Laplace equation:

$$\Psi_{x^*x^*} + \Psi_{y^*y^*} + \Psi_{z^*z^*} = 0, \tag{9}$$

where subscripts are derivatives. The surface ($z = 0$) and top ($z^* = h^*$) boundary conditions are that the vertical velocity is zero [Eqs. (10) and (11)]. The boundary conditions on the surface between the levels ($z^* = 1$) are that the pressure and vertical velocity are continuous [Eqs. (12) and (13)]. The boundary conditions are expressed as

$$(\Psi_{z^*t^*} - \Psi_{x^*})|_{z^*=0} = 0, \tag{10}$$

$$(\Psi_{z^*t^*} - \Psi_{z^*x^*} - \gamma^*\Psi_{z^*x^*} + h^*\gamma^*\Psi_{z^*x^*} - \gamma^*\Psi_{x^*})|_{z^*=h^*} = 0, \tag{11}$$

$$\Psi|_{z^*=1^-} = \Psi|_{z^*=1^+}, \quad \text{and} \tag{12}$$

$$(\Psi_{z^*t^*} + \Psi_{z^*x^*} - \Psi_{x^*})|_{z^*=1^-} = (\Psi_{z^*t^*} + \Psi_{z^*x^*} - \gamma^*\Psi_{x^*})|_{z^*=1^+}. \tag{13}$$

In Fig. 16a the zonal velocity profiles of three different cases are plotted, and in Fig. 16b the corresponding growth rates are plotted. The solid line has a uniform shear as in the Eady problem ($\gamma = 0.002\,\mathrm{s}^{-1}$), while the dotted line and dashed line show the solutions for cases that the mean shear is equal to the solid line, but the shear in the upper and lower levels are different ($\gamma_u = 0.002 \pm 0.0005\,\mathrm{s}^{-1}$ and $\gamma_l = 0.002 \mp 0.0005\,\mathrm{s}^{-1}$). The growth rates of the two cases

of nonuniform shear are identical, hence it does not assist in differentiating between the contribution of the upper- and lower-level shear. Furthermore, this example shows that the mean shear does not determine the growth rate since the nonuniform cases has a larger growth rate than the uniform shear case.

To better understand the relative importance of the lower and upper levels, we choose a reference state that has nonuniform shear (solid line in Fig. 16c). This case is analogous to the atmospheric state where the Eady growth rate is larger in the upper troposphere as in our simulations. The reference was modified such that the shear was reduced by $0.0005\,s^{-1}$ in each layer separately, thus the mean shear for the two cases is equal, but in one case the upper level has the same shear as the reference (Fig. 16c, dashed line), and in the second case the lower section has the same shear as the reference (Fig. 16c, dotted line). Figure 16d shows that the upper-layer change affects the growth rate more significantly (the maximum of the dotted line is below the maximum of the dashed line). For wide range of parameters tested, it was found that when the shear is not uniform in the two regions, changing the shear in the region where the shear is larger affects the growth rate more than changing the shear in the region where the shear is smaller.[12]

We stress that the 1D problem can assist understanding the linear dynamics but does not take into account any nonlinear dynamics. Furthermore, the results in this study are different than previous results by Held and O'Brien (1992) and Pavan (1996), which used a QG model and found that EKE and eddy fluxes are more sensitive to changes in lower-level baroclinicity. In the three-level linear model used by Held and O'Brien (1992) they show that the growth rate of disturbances increases as the shear is more concentrated in the lower level, and decreases as the shear is more concentrated in the upper level, and they demonstrate that their QG model follows this result. The reason that their linear model gives a different prediction than the piecewise Eady model presented here is that they included the β effect. The β effect leads to a behavior that near linear shear, the growth rate increases as the shear is more concentrated in the lower level and decreases as the shear is more concentrated in the upper level. However, this qualitative behavior of the growth rate is only correct in cases that there is no large concentration of shear (close to linear shear), which are the cases they investigated. In cases where the shear (or baroclinicity) is far from vertically uniform, one can show in a linear model (as we show in a forthcoming paper) that the growth rate increases as the shear is more concentrated in a specific region—as was shown qualitatively in the simple Eady model in this section. The qualitative reason that the EKE is more sensitive to changes in upper baroclinicity in the simulations presented in this study is that the baroclinicity of the reference state we use is concentrated in the upper troposphere. Other studies such as Lunkeit et al. (1998) that found larger eddy sensitivity to lower baroclinicity, used a much less idealized framework, and also included temperature changes in the tropics such that it is difficult to equate the results of this study to their study.

b. *Sensitivity to diabatic heating*

The method presented in this study permits simulating a prescribed temperature field. However, it is possible that simulations with different parameters have the same temperature field but different eddy activity (see EKE in Fig. 2). Therefore, an essential issue is to determine to what extent the temperature profile determines the circulation. In classical eddy–mean flow problems the temperature profile is assumed to be given and the circulation properties are derived from the given temperature field (e.g., the Eady problem). The approach used in this study was similar. Eddy activity responses to different temperature profiles were studied. This approach was motivated by the assumption that eddy activity differences are primarily caused by the different temperature profiles, with the underlying assumption that the diabatic forcing plays a direct role in determining the temperature profile; however, the diabatic forcing does not play a direct role in determining the eddy properties. If the diabatic forcing has a direct effect on the circulation, the knowledge regarding temperature distribution alone is not enough to deduct robust conclusions regarding the circulation. For example, the result that in some of our simulations, the EKE was decreased (increased) as a response to increased (decreased) lower-tropospheric temperature gradient suggests that the temperature gradient (or Eady growth rate) may not be a sufficient measure for instabilities, and the diabatic heating plays an important role as well.

We note that the result that the upper-tropospheric temperature gradient affects eddy activity more than the lower-tropospheric temperature gradient occurs also when using a the standard Held and Suarez (1994) relaxation temperature profile. Figures 1a–c shows the temperature profile change to the relaxation temperature change plotted in Figs. 1d–f. Figures 1g–i shows the EKE response to these changes. Despite the fact that the temperature changes were much larger in the simulations where the

[12] The reason we choose to show the results in terms of the real parameters is that when rescaling the variables, the phase velocity is rescaled by the shear of one layer. Since we want to change each shear separately, the scale of the phase velocity would be different for different cases.

mid- or lower-tropospheric temperatures were modified, the EKE response is on the same order of magnitude in all simulations. This implies that also in these simulations, where our method for determining the relaxation temperature was not used, the eddy activity is affected mostly from the temperature gradient in the upper troposphere.[13]

6. Conclusions

In this study the relative importance of the upper- and lower-tropospheric meridional temperature gradients for the magnitude of EKE and eddy fluxes is investigated. The response of eddies to changes in the vertical structure of the temperature gradient is especially interesting, since global circulation models suggest that as a result of greenhouse warming, the lower-tropospheric temperature gradient will decrease, whereas the upper-tropospheric temperature gradient will increase.

An idealized GCM with a Newtonian cooling scheme allowed us to control the temperature profile to a good degree, which in turn allowed a comparison between cases where the lower- and upper-tropospheric temperature gradients were modified separately. Consistently, it was found that the eddy activity is affected mostly from changes in the upper temperature gradient changes. We hypothesized that a possible reason for the importance of the upper-tropospheric levels on the eddy activity is a consequence of the vertical structure of the Eady growth rate, which in our runs (as well as in the atmosphere) is maximal in the upper-tropospheric levels. It was demonstrated that in a simple 1D Eady-like problem, shear changes in levels where the shear is large, have a larger effect on the growth rate than shear changes in levels which the shear is smaller.

This study suggests that in a global warming scenario, the effects of an increased upper-troposphere meridional temperature gradient will dominate the response of eddy activity resulting in a larger EKE. This is consistent with the results of Wu et al. (2011) who used a more complex GCM. It should be noted that our conclusions rely on idealized temperature changes, while the temperature changes that are predicted to occur in a global warming scenario have a more complicated structure.

It is found that in some cases when the lower temperature gradient is increased (decreased), the eddy kinetic energy decreased (increased). We speculate that this result might be related to the midwinter minimum observed in EKE above the Pacific Ocean. It is demonstrated that the midwinter minimum in EKE can be reproduced by simulating a zonally symmetric temperature profile that is Pacific-like.

Acknowledgments. We thank Rei Chemke, Hilla Afargan, and Eli Tziperman for important discussions regarding this work. This research has been supported by an EU-FP7 Marie Curie Grant (CIG-304202), and the Israeli Science Foundation (Grants 1310/12 and 1859/12).

APPENDIX

Heating Applied in z Coordinates versus σ Coordinates

In the schemes described in sections 2c and 2d, the vertical interval of the modifications applied to the temperature/heating field were taken in σ coordinates. Namely, the modifications at different levels were taken in the same interval in σ coordinates ($\delta\sigma$ was the same for different choices of σ_c). This choice changes the temperature for the same amount of mass at different levels. Another possibility is to change the temperature/heating profile in such a way that the vertical interval of change will be similar in z coordinates.

One possible argument to prefer z coordinates rather than σ coordinates is that changes in the meridional temperature gradients in the same σ intervals will lead to different changes in the zonal wind. This is because thermal wind balance in pressure coordinates is expressed as $p\partial_p u_g = (R_d/f)\partial_y T$, where u_g is the geostrophic zonal wind, p is the pressure, R_d is the gas constant, f is the Coriolis parameter, y is the meridional coordinate, and T is the temperature. As long as the simulation obeys thermal wind balance, it is expected that the change in the zonal wind will be larger in cases where the upper troposphere was modified, because of the pressure term p that appears on the LHS. One might expect that the changes in eddy activity will be related to the changes in the mean geostrophic wind, which might explain why gradient temperature changes in the upper troposphere cause larger changes in eddy activity than gradient temperature changes in the lower troposphere. To test this hypothesis, simulations were performed such that the vertical interval

[13] Notice that the temperature response to modifications in the relaxation temperature is much larger in the lower troposphere than the upper troposphere (Fig. 1). Since the diabatic heating is proportional to $(T_{\text{relax}} - T)/\tau$, the diabatic forcing added will be larger in the upper troposphere because the difference $T_{\text{relax}} - T$ is larger in the upper troposphere than the lower troposphere. An assumption that eddy activity is affected also by the diabatic heating and not only by the temperature field, could be consistent with most of our results.

of temperature modifications in z coordinates was similar (for $\sigma_c = 0.65, 0.85$, we used $\delta\sigma = 0.15, 0.2$, respectively). The results of these simulations (not shown) show that the response of the EKE change is larger when the upper temperature gradient is modified, which is consistent with the results presented in section 3.

REFERENCES

Ait-Chaalal, F., and T. Schneider, 2015: Why eddy momentum fluxes are concentrated in the upper troposphere. *J. Atmos. Sci.*, **72**, 1585–1604, doi:10.1175/JAS-D-14-0243.1.

Alexeev, V. A., 2003: Sensitivity to CO_2 doubling of an atmospheric GCM coupled to an oceanic mixed layer: A linear analysis. *Climate Dyn.*, **20**, 775–787, doi:10.1007/s00382-003-0312-x.

Bengtsson, L., and K. I. Hodges, 2006: Storm tracks and climate change. *J. Climate*, **19**, 3518–3543, doi:10.1175/JCLI3815.1.

Blumen, W., 1979: On short-wave baroclinic instability. *J. Atmos. Sci.*, **36**, 1925–1933, doi:10.1175/1520-0469(1979)036<1925:OSWBI>2.0.CO;2.

Bourke, W., 1974: A multi-level spectral model. I. Formulation and hemispheric integrations. *Mon. Wea. Rev.*, **102**, 687–701, doi:10.1175/1520-0493(1974)102<0687:AMLSMI>2.0.CO;2.

Bintanja, R., R. G. Graversen, and W. Hazeleger, 2011: Arctic winter warming amplified by the thermal inversion and consequent low infrared cooling to space. *Nat. Geosci.*, **4**, 758–761, doi:10.1038/ngeo1285.

Cai, M., 2005: Dynamical amplification of polar warming. *Geophys. Res. Lett.*, **32**, L22710, doi:10.1029/2005GL024481.

——, 2006: Dynamical greenhouse plus feedback and polar warming amplification. Part I: A dry radiative-transportive climate model. *Climate Dyn.*, **26**, 661–675, doi:10.1007/s00382-005-0104-6.

Chang, E. K. M., 2001: GCM and observational diagnoses of the seasonal and interannual variations of the Pacific storm track during the cool season. *J. Atmos. Sci.*, **58**, 1784–1800, doi:10.1175/1520-0469(2001)058<1784:GAODOT>2.0.CO;2.

——, 2006: An indealized nonlinear model of the Northern Hemisphere winter storm tracks. *J. Atmos. Sci.*, **63**, 1818–1839, doi:10.1175/JAS3726.1.

Chen, G., I. M. Held, and W. A. Robinson, 2007: Sensitivity of the latitude of the surface westerlies to surface friction. *J. Atmos. Sci.*, **64**, 2899–2915, doi:10.1175/JAS3995.1.

Eady, E. T., 1949: Long waves and cyclonic waves. *Tellus*, **1A**, 33–52, doi:10.1111/j.2153-3490.1949.tb01265.x.

Ferrari, R., and M. Nikurashin, 2010: Suppression of eddy diffusivity across jets in the southern Pacific. *J. Phys. Oceanogr.*, **40**, 1501–1519, doi:10.1175/2010JPO4278.1.

Green, J. G. A., 1970: Transfer properties of the large scale eddies and the general circulation of the atmosphere. *Quart. J. Roy. Meteor. Soc.*, **96**, 157–185, doi:10.1002/qj.49709640802.

Hall, N. M. J., and P. D. Sardeshmukh, 1998: Is the time-mean Northern Hemisphere flow baroclinically unstable? *J. Atmos. Sci.*, **55**, 41–56, doi:10.1175/1520-0469(1998)055<0041:ITTMNH>2.0.CO;2.

——, B. J. Hoskins, and P. J. Valdes, 1994: Storm tracks in a high-resolution GCM with doubled carbon dioxide. *Quart. J. Roy. Meteor. Soc.*, **120**, 1209–1230, doi:10.1002/qj.49712051905.

Hansen, J. E., A. Lacis, D. Rind, G. Russel, P. Stone, I. Fung, R. Ruedy, and J. Lerner, 1984: Climate sensitivity: Analysis of feedback mechanisms. *Climate Processes and Climate Sensitivity, Geophys. Monogr.*, Vol. 29, Amer. Geophys. Union, 130–163.

Harnik, N., and E. K. M. Chang, 2004: The effects of variations in jet width on the growth of baroclinic waves: Implications for midwinter Pacific storm track variability. *J. Atmos. Sci.*, **61**, 23–40, doi:10.1175/1520-0469(2004)061<0023:TEOVIJ>2.0.CO;2.

Hartmann, D. L., and P. Zuercher, 1998: Response of baroclinic life cycles to barotropic shear. *J. Atmos. Sci.*, **55**, 297–313, doi:10.1175/1520-0469(1998)055<0297:ROBLCT>2.0.CO;2.

Held, I. M., 1978: The vertical scale of an unstable baroclinic wave and its importance for eddy heat flux parameterizations. *J. Atmos. Sci.*, **35**, 572–576, doi:10.1175/1520-0469(1978)035<0572:TVSOAU>2.0.CO;2.

——, 1993: Large-scale dynamics and global warming. *Bull. Amer. Meteor. Soc.*, **74**, 228–242, doi:10.1175/1520-0477(1993)074<0228:LSDAGW>2.0.CO;2.

——, and E. O'Brien, 1992: Quasigeostrophic turbulence in a three-layer model: Effects of vertical structure in the mean shear. *J. Atmos. Sci.*, **49**, 1861–1870, doi:10.1175/1520-0469(1992)049<1861:QTIATL>2.0.CO;2.

——, and M. J. Suarez, 1994: A proposal for the intercomparison of the dynamical cores of atmospheric general circulation models. *Bull. Amer. Meteor. Soc.*, **75**, 1825–1830, doi:10.1175/1520-0477(1994)075<1825:APFTIO>2.0.CO;2.

Hoskins, B. J., and P. J. Valdes, 1990: On the existence of storm-tracks. *J. Atmos. Sci.*, **47**, 1854–1864, doi:10.1175/1520-0469(1990)047<1854:OTEOST>2.0.CO;2.

Ioannou, P., and R. S. Lindzen, 1986: Baroclinic instability in the presence of barotropic jets. *J. Atmos. Sci.*, **43**, 2999–3014, doi:10.1175/1520-0469(1986)043<2999:BIITPO>2.0.CO;2.

Iwasaki, T., and C. Kodama, 2011: How does the vertical profile of baroclinicity affect the wave instability? *J. Atmos. Sci.*, **68**, 863–876, doi:10.1175/2010JAS3609.1.

James, I. N., 1987: Suppression of baroclinic instability in horizontally sheared flows. *J. Atmos. Sci.*, **44**, 3710–3720, doi:10.1175/1520-0469(1987)044<3710:SOBIIH>2.0.CO;2.

——, and L. J. Gray, 1986: Concerning the effect of surface drag on the circulation of a baroclinic planetary atmosphere. *Quart. J. Roy. Meteor. Soc.*, **112**, 1231–1250, doi:10.1002/qj.49711247417.

Kodama, C., and T. Iwasaki, 2009: Influence of the SST rise on baroclinic instability wave activity under an aquaplanet condition. *J. Atmos. Sci.*, **66**, 2272–2287, doi:10.1175/2009JAS2964.1.

Lorenz, D. J., and D. L. Hartmann, 2001: Eddy–zonal flow feedback in the Southern Hemisphere. *J. Atmos. Sci.*, **58**, 3312–3327, doi:10.1175/1520-0469(2001)058<3312:EZFFIT>2.0.CO;2.

Lorenz, E. N., 1955: Available potential energy and the maintenance of the general circulation. *Tellus*, **7A**, 157–167, doi:10.1111/j.2153-3490.1955.tb01148.x.

Lu, J., and M. Cai, 2010: Quantifying contributions to polar warming amplification in an idealized coupled general circulation model. *Climate Dyn.*, **34**, 669–687, doi:10.1007/s00382-009-0673-x.

Lunkeit, F., L. Fraedrich, and S. E. Bauer, 1998: Storm tracks in warmer climate: Sensitivity studies with a simplified global circulation model. *Climate Dyn.*, **14**, 813–826, doi:10.1007/s003820050257.

Manabe, S., and R. T. Wetherald, 1975: The effects of doubling the CO_2 concentration on the climate of a general circulation model. *J. Atmos. Sci.*, **32**, 3–15, doi:10.1175/1520-0469(1975)032<0003:TEODTC>2.0.CO;2.

——, and ——, 1980: On the distribution of climate change resulting from an increase in CO_2 content of the atmosphere. *J. Atmos. Sci.*, **37**, 99–118, doi:10.1175/1520-0469(1980)037<0099:OTDOCC>2.0.CO;2.

Meehl, G. A., and Coauthors, 2007: Global climate projections. *Climate Change 2007: The Physical Science Basis*, S. Solomon et al., Eds., Cambridge University Press, 747–845.

Merlis, T. M., and T. Schneider, 2009: Scales of linear baroclinic instability and macroturbulence in dry atmospheres. *J. Atmos. Sci.*, **66**, 1821–1833, doi:10.1175/2008JAS2884.1.

Muller, J., 1991: Baroclinic instability in a two-layer, vertically semi-infinite domain. *Tellus*, **43A**, 275–284, doi:10.1034/j.1600-0870.1991.t01-4-00003.x.

Nakamura, H., 1992: Midwinter suppression of baroclinic wave activity in the Pacific. *J. Atmos. Sci.*, **49**, 1629–1642, doi:10.1175/1520-0469(1992)049<1629:MSOBWA>2.0.CO;2.

O'Gorman, P. A., 2010: Understanding the varied response of the extratropical storm tracks to climate change. *Proc. Natl. Acad. Sci. USA*, **107**, 19 176–19 180, doi:10.1073/pnas.1011547107.

——, 2015: Precipitation extremes under climate change. *Curr. Climate Change Rep.*, **1**, 49–59, doi:10.1007/s40641-015-0009-3.

——, and T. Schneider, 2008: Energy in midlatitude transient eddies in idealized simulations of changed climates. *J. Climate*, **21**, 5797–5806, doi:10.1175/2008JCLI2099.1.

Park, H., J. C. H. Chiang, and S. Son, 2010: The role of the central Asian mountains on the midwinter suppression of North Pacific storminess. *J. Atmos. Sci.*, **67**, 3706–3720, doi:10.1175/2010JAS3349.1.

Pavan, V., 1996: Sensitivity of a multi-layer quasi-geostrophic beta-channel to the vertical structure of the equilibrium meridional temperature gradient. *Quart. J. Roy. Meteor. Soc.*, **122**, 55–72, doi:10.1002/qj.49712252904.

Pedlosky, J., 1987: *Geophysical Fluid Dynamics*. Springer, 710 pp.

Penny, S., G. H. Roe, and D. S. Battisti, 2010: The source of the midwinter suppression in storminess over the North Pacific. *J. Climate*, **23**, 634–648, doi:10.1175/2009JCLI2904.1.

Schneider, E. K., R. L. Lindzen, and B. P. Kirtman, 1997: A tropical influence on global climate. *J. Atmos. Sci.*, **54**, 1349–1358, doi:10.1175/1520-0469(1997)054<1349:ATIOGC>2.0.CO;2.

Smagorinsky, J., S. Manabe, and J. L. Holloway Jr., 1965: Numerical results from a nine-level general circulation model of the atmosphere. *Mon. Wea. Rev.*, **93**, 727–768, doi:10.1175/1520-0493(1965)093<0727:NRFANL>2.3.CO;2.

Sobel, A. H., J. Nilsson, and L. M. Polvani, 2001: The weak temperature gradient approximation and balanced tropical moisture waves. *J. Atmos. Sci.*, **58**, 3650–3665, doi:10.1175/1520-0469(2001)058<3650:TWTGAA>2.0.CO;2.

Stephenson, D. B., and I. M. Held, 1993: GCM response of northern winter stationary waves and storm tracks to increasing amounts of carbon dioxide. *J. Climate*, **6**, 1859–1870, doi:10.1175/1520-0442(1993)006<1859:GRONWS>2.0.CO;2.

Thompson, D. E. J., and E. A. Barnes, 2014: Periodic variability in the large-scale Southern Hemisphere atmospheric circulation. *Science*, **343**, 641–645, doi:10.1126/science.1247660.

Vallis, G. K., 2006: *Atmospheric and Oceanic Fluid Dynamics*. Cambridge University Press, 770 pp.

——, P. Zurita-Gotor, C. Cairns, and J. Kidston, 2014: Response of the large-scale structure of the atmosphere to global warming. *Quart. J. Roy. Meteor. Soc.*, **141**, 1479–1501, doi:10.1002/qj.2456.

Wittman, M. A. H., A. J. Charlton, and L. M. Polvani, 2007: The effect of lower stratospheric shear on baroclinic instability. *J. Atmos. Sci.*, **64**, 479–496, doi:10.1175/JAS3828.1.

Wu, Y., M. Ting, R. Seager, H.-P. Huang, and M. A. Cane, 2011: Changes in storm tracks and energy transports in a warmer climate simulated by the GFDL CM2.1 model. *Climate Dyn.*, **37**, 53–72, doi:10.1007/s00382-010-0776-4.

Yin, J. H., 2005: A consistent poleward shift of the storm tracks in simulations of 21st century climate. *Geophys. Res. Lett.*, **32**, L18701, doi:10.1029/2005GL023684.